Atmos. Chem. Phys. Discuss., 15, 12069–12105, 2015
www.atmos-chem-phys-discuss.net/15/12069/2015/
doi:10.5194/acpd-15-12069-2015

Atmospheric Chemistry and Physics Discussions

Use of criteria pollutants, active and passive mercury sampling, and receptor modeling to understand the chemical forms of gaseous oxidized mercury in Florida

J. Huang[1], M. B. Miller[1], E. Edgerton[2], and M. S. Gustin[1]

[1]Department of Natural Resources and Environmental Sciences, University of Nevada-Reno,1664 N. Virginia Street, Reno, NV, 89557, USA
[2]Atmospheric Research and Analysis, Inc., 410 Midenhall Way, Cary, North Carolina 27513, USA

Received: 10 February 2015 – Accepted: 27 March 2015 – Published: 22 April 2015

Correspondence to: M. S. Gustin (mgustin@cabnr.unr.edu)

Published by Copernicus Publications on behalf of the European Geosciences Union.

Abstract

The highest mercury (Hg) wet deposition in the United States (US) occurs along the Gulf of Mexico, and in the southern and central Mississippi River Valley. Gaseous oxidized Hg (GOM) is thought to be a major contributor due to its high water solubility and reactivity. Therefore, it is critical to understand the concentrations, potential for wet and dry deposition, and GOM compounds present in the air. Concentrations and dry deposition fluxes of GOM were measured at Outlying Landing Field (OLF), Florida, using a Tekran® 2537/1130/1135, and active and passive samplers using cation-exchange and nylon membranes. Relationships with Tekran® derived data must be interpreted with caution, since GOM concentrations can be biased low depending on the chemical compounds in air, and interferences with water vapor and ozone. Only gaseous elemental Hg and GOM are discussed here since the PBM measurement uncertainties are higher. Criteria air pollutants were concurrently measured and Tekran® data were assessed along with these using Principal Component Analysis to identify associations among air pollutants. Based on the diel pattern, high GOM concentrations at this site were associated with fossil fuel combustion and gas phase oxidation during the day, and gas phase oxidation and transport in the free troposphere. The ratio of GEM/CO at OLF ($0.008\,ng\,m^{-3}\,ppbv^{-1}$) was much higher than the numbers reported for the Western United States and central New York for domestic emissions or biomass burning ($0.001\,ng\,m^{-3}\,ppbv^{-1}$), which we suggest is indicative of a marine boundary layer source.

Results from nylon membranes with thermal desorption analyses suggest five potential GOM compounds exist in this area, including $HgBr_2$, HgO, $Hg(NO_3)_2$, $HgSO_4$, and an unknown compound. This indicates that the site is influenced by different gaseous phase reactions and sources. A high GOM event related to high CO but average SO_2 suggests the air parcels moved from the free troposphere and across Arkansas, Mississippi, and Alabama at low elevation (< 300 m) using back trajectory analysis. We hypothesize this is due to subsidence of Hg containing air from the free troposphere.

ACPD
15, 12069–12105, 2015

It is difficult to fully understand GOM dry deposition processes without knowing the actual GOM compounds, and their corresponding physicochemical properties, such as the Henry's Law constant. Overall, measured GOM dry deposition at this site ranged from 4–23 % of total Hg wet deposition. The Aerohead sampling system for dry deposition captures primarily GOM since it would only collect fine particulate bound Hg by way of diffusion.

1 Introduction

Mercury (Hg) has been classified as a persistent, bioaccumulative toxin (PBT) (UNEP, 2013), and deposition from the atmosphere is considered the dominant pathway by which Hg enters remote ecosystems (Lindberg et al., 2007). In some areas, scavenging by precipitation controls atmospheric Hg removal processes, such as the Southeastern United States (US), where precipitation amounts are high (Prestbo and Gay, 2009). However, wet deposition concentrations are not necessarily correlated with precipitation amounts > 81 mm and deposition has not decreased with emission reductions as coal combustion facilities in the region have implemented control technologies (Prestbo and Gay, 2009). A contributing factor to wet deposition in the Gulf Coast area may be related to high atmospheric convection during thunderstorms and scavenging of gaseous oxidized Hg (GOM) from the free troposphere (Nair et al., 2013), and down mixing of air with high GOM from the free troposphere (cf. Gustin et al., 2012). An additional concern is that the Tekran® system measurement does not quantify all GOM (see discussion below), and this may result in underestimation of GOM in the atmosphere. Since GOM is considered an important form that can be rapidly removed from the atmosphere due to high water solubility (Lindberg et al., 2007); it is important to understand both atmospheric concentrations and chemistry (i.e. specific chemical compounds).

The Atmospheric Mercury Network (AMNet) uses the Tekran® system (Gay et al., 2013) to measure ambient air Hg concentrations, including gaseous elemental Hg

ACPD
15, 12069–12105, 2015

(GEM), GOM, and fine-particulate bound Hg (PBM, particle size < 2.5 µm). There are four AMNet sites in the Southeastern US, including AL19, GA40, MS12, and FL96 (Gay et al., 2013). The Tekran® system has been used since 2002 (Landis et al., 2002) to understand atmospheric reactions, behavior, and transport of GOM. However, GOM concentrations measured by the Tekran® system have recently been demonstrated to be significantly lower than ambient values due to lack of efficient collection of all GOM compounds, and/or reduction of GOM on the KCl-coated denuder by ozone and humidity (Ambrose et al., 2013; Gustin et al., 2013; Huang et al., 2013; Lyman et al., 2010; McClure et al., 2014). New methods, including a differential method, University of Washington Detector for Oxidized Hg (GOM method detection limit 80 $pg\,m^{-3}$; Ambrose et al., 2013) (DOHGS), and cation exchange membranes (Ambrose et al., 2013; Huang et al., 2013; Lyman and Jaffe, 2012) have demonstrated that there are higher concentrations than those measured by the Tekran® in the laboratory and in the field at high elevation (Gustin et al., 2013). Additionally, use of the University of Nevada-Reno (UNR) active system that collects GOM on nylon membranes in tandem with cation exchange membranes allows for compounds to be identified, and the concentration of GOM determined, respectively (Huang et al., 2013).

Mercury has been studied in Florida for many years, initially because of the high concentrations measured in fish and the Florida Panther. Dvonch et al. (1999) concluded a major Hg source in South Florida (Broward County and Dade County, 1995–1996) were medical waste incinerators, and this study informed decisions regarding small individual medical waste incinerators. Detailed work has been done in Florida at Everglades National Park and the municipalities of Pensacola, Davie (near Fort Lauderdale) and Tampa Bay, to understand atmospheric Hg deposition and concentrations. These studies applied water and cation-exchange membrane surrogate surfaces, passive samplers, Tekran® speciation systems, and semi-continuous aerosol samplers (Gustin et al., 2012; Marsik et al., 2007; Pancras et al., 2011; Peterson et al., 2012). Annual GEM, GOM, and PBM ambient air concentrations in these areas, as measured by the Tekran® system, were 1.2–1.4 $ng\,m^{-3}$, 2–7 $pg\,m^{-3}$, and 2–3 $pg\,m^{-3}$, respec-

ACPD
15, 12069–12105, 2015

tively (Peterson et al., 2012), and reported Hg dry and wet deposition ranged from 1.8–4.7 and 13.5–20.1 $\mu g\,m^{-2}\,yr^{-1}$, respectively (Marsik et al., 2007; Peterson et al., 2012; Prestbo and Gay, 2009). Long-term GEM and GOM concentrations as measured by the Tekran® system have declined; however, PBM concentrations increased after 2009. Given the uncertainties associated with the GOM and PBM measurements it is possible that increasing PBM could be GOM compounds.

Engle et al. (2008) stated that elevated GOM concentrations during the day at a site near Weeks Bay, Alabama, in April and May were related to high average ozone concentrations and solar radiation, and the marine boundary was not a significant GOM source. Since the Tekran® system does not measure all compounds of GOM with equal efficiency; it is possible that they were not capturing all the GOM. They indicated, based on limited data, a significant component of PM was greater than 2.5 µm and this size fraction is not measured by the Tekran® system. Gridded frequency distribution with back trajectories, and EPA UNMIX, have been used to understand potential sources of atmospheric Hg concentrations in Florida (Gustin et al., 2012; Pancras et al., 2011). Gustin et al. (2012) investigated sources in Tampa, Pensacola, and Davie. They found direct atmospheric Hg sources in Florida included local electric power generation plants, industry, and the free troposphere, and indirect sources included mobile and point sources of oxidants that could transform GEM to reactive Hg (RM = GOM + PBM). Weiss-Penzias et al. (2011) concluded that two different sources, including free troposphere and coal-fired power plants, influenced GOM dry deposition at OLF. Landing et al. (2010) indicated that roughly 20 % of Hg in wet deposition in Florida was attributed to regional coal combustion and there was no evidence of a change in wet deposition after the installation of scrubbers on Plant Crist. This indicates that a local influence from the power plant was not detectable supporting conclusions in Gustin et al. (2012). In summary, atmospheric Hg in Florida has many sources that range from local to regional and global in scale, and there has been disagreement about the most important sources.

ACPD
15, 12069–12105, 2015

In this work, Hg was measured concurrently with various trace gases (CO, O_3, SO_2, NO_x, NO_y) and meteorological data at Outlying Landing Field (OLF) located ~ 15 km NW of Pensacola, Florida. Air GEM/GOM/PBM concentrations were measured by the Tekran® 2537/1130/1135 system. Here we focus primarily on measurement of GEM and GOM, if we add PBM, the uncertainties increase. Tentative air pollutant sources were identified using these data analyzed with Principal Component Analysis (PCA).

We applied the Aerohead sampler developed Lyman et al. (2007, 2009) for measurement of dry deposition of GOM. The surrogate surface used is an aerodynamic sampler housing a cation exchange membrane that collects particles and gases via diffusion and thus, at OLF, collects primarily GOM. We also used the UNR active system for measurement of GOM concentrations and chemistry. Cation-exchange membranes in this system are used to understand GOM concentration in the atmosphere, and the nylon membranes are used to determine the chemistry of potential GOM compounds (cf. Huang et al., 2013). Finally, GOM dry deposition fluxes were calculated using deposition velocities determined from multi-resistance model with ambient air GOM concentrations from the Tekran® system (adjusted by a factor of 3 due to uncertainties in the Tekran® system; cf. Huang and Gustin, 2015a) and compared to those obtained using surrogate surface data. The results were used to estimate the dry deposition velocity for the potential GOM compounds observed. The hypothesis for this work was that GOM compounds vary over time, and this is due to different compounds produced by different sources and processes. Additionally, because different compounds will have different Henry's law constants this will result in different dry deposition velocities and dry deposition flux.

ACPD
15, 12069–12105, 2015

2 Methods

2.1 Field site

The sampling site was located at the Outlying Landing Field (OLF, 30.550° N, 87.374° W, 44 m a.s.l.). The closest major Hg emission source is a coal-fired power plant (Plant Crist) northeast of the site (Fig. 1). This area has been used for atmospheric Hg research in previous studies (Caffrey et al., 2010; Engle et al., 2008; Gustin et al., 2012; Peterson et al., 2012; Weiss-Penzias et al., 2011). OLF is a coastal site (~ 25 km away from Gulf of Mexico) influenced by sea breezes especially during the summer (Engle et al., 2008; Gustin et al., 2012).

2.2 Sampling methods

Passive box and Aerohead samplers were deployed bi-weekly from June 2012 to March 2014. The UNR active samplers were deployed biweekly from March 2013 to March 2014. Atmospheric Hg concentrations, including GEM, GOM, and PBM, were measured using a Tekran® system (model 2357/1130/1135, Tekran® Instrument Corp., Ontario, Canada) that was operated with one-hour sampling and one hour desorption with blanks of 0.1 ng m^{-3}, 1.5, and 1.5 pg m^{-3}, respectively. Gaseous oxidized Hg concentrations were also measured using the UNR active system with 3 sets of two in-series 47 mm cation-exchange membranes (ICE450, Pall Corp., MI, USA) and 3 sets of nylon membranes (0.2 µm, Cole-Parmer, IL, USA). Based on the sampler design, it is thought this method collects primarily GOM (cf. Huang et al., 2013). Detailed information on the UNR active GOM sampling system can be found in Huang et al. (2013). Criteria air pollutants and meteorological data, including CO, SO_2, O_3, $PM_{2.5}$, NO, NO_2, NO_y, temperature, relative humidity, wind speed, wind direction, pressure, solar radiation, and precipitation were available at this site for the sampling period, see Peterson et al. (2012) for detailed information on these measurements.

ACPD
15, 12069–12105, 2015

Passive samplers and Aeroheads were prepared at UNR, and two sets of samples were packed in a thermal isolated cooler shipped back and forth between the laboratory and site. Cation-exchange and nylon membranes for the active system were pre-cut at UNR and stored in acid cleaned glass jars and packed in double Ziploc® bags. Passive, Aerohead, and active samplers were deployed by the site operator every two weeks. After collection, all membranes were stored in acid clean jars in double Ziploc® bags and sent back to UNR. Samples were stored in a freezer (−22 °C) at UNR until analyzed. Cation-exchange membranes were then digested and analyzed following EPA Method 1631 E (Peterson et al., 2012), and nylon membranes were first thermally desorbed and then analyzed using EPA Method 1631 E (Huang et al., 2013). Cation-exchange membrane blanks for passive box, Aerohead, and active samplers were 0.32 ± 0.15 (n = 38), 0.40 ± 0.18 (n = 42), 0.37 ± 0.26 (n = 77) ng, respectively; and for nylon membranes used in the active system blanks were 0.03 ± 0.03 (n = 69) ng. Therefore, method detection limits (MDL, 3-sigma) for two-week sampling time (336 h) were 1.4 pg h^{-1}, 0.13 ng m^{-2} h^{-1} for uptake rate and dry deposition, respectively. For the active membrane system, the Hg amount on the back-up filters and blanks were not significantly different (cation-exchange membrane: 0.4 ± 0.3 vs. 0.4 ± 0.3 ng; nylon membrane: 0.03 ± 0.03 vs. 0.02 ± 0.02 ng); therefore, the back-up filters were included in the calculation of the bi-weekly blanks. The biweekly MDL (336 h) for active system with cation-exchange and nylon membranes were 1.8–66.9 pg m^{-3} (mean: 23.8 pg m^{-3}) and 0.01–14.6 pg m^{-3} (mean: 2.1 pg m^{-3}), respectively. Bi-weekly MDL was calculated from 3 times the standard deviation of bi-weekly blanks. All samples were corrected by subtracting the blank for the corresponding two-week period.

Hourly Tekran®, criteria air pollutants, and meteorological data were managed and validated by Atmospheric Research and Analysis, Inc.; these were then averaged into two-week intervals to merge with the membrane measurements.

ACPD
15, 12069–12105, 2015

2.3 Principal component analysis

Principal Component Analysis is a tool that allows for reduction of a large data set to one that is smaller, and converts a set of observations of possibly correlated variables into a set of factors with linearly uncorrelated variables (Belis et al., 2013; Jackson, 1991). Varimax rotations are used to maximize the variance of the squared loadings of a factor and were applied to separate all factors. Hourly air concentrations and meteorological data were merged to Tekran® sampling hour; data below MDL and missing data were replaced by half of MDL and mean, respectively. To standardize data, they were subtracted by corresponding mean and divided by standard deviation before PCA. Data included mixing ratios of CO, SO_2, O_3, NO, NO_2, NO_y, concentrations of $PM_{2.5}$, temperature, relative humidity, wind speed, pressure, solar radiation, and precipitation. PCA factor scores were calculated using Statistica 7.0 (StatSoft, Inc.).

2.4 Dry deposition model

After potential GOM compounds in ambient air at OLF were identified (using nylon membranes with thermal desorption), dry deposition rates associated with the specific compounds (determined using the surrogate surface) were then applied in a multiple-resistance model modified from Zhang et al. (2003) to calculate Hg dry deposition velocities. Modeled Hg dry deposition fluxes were then determined using calculated dry deposition velocities multiplied using adjusted GOM ambient concentrations measured by the Tekran® system. GOM ambient concentrations from Tekran® measurements were adjusted using each compound's corresponding correction factor, derived in the laboratory through comparison of cation-exchange membrane measured concentrations vs. those measured using the KCl-denuder (average: 3. $HgBr_2$: 1.6, $HgCl_2$: 2.4, $HgSO_4$: 2.3, HgO : 3.7, and $Hg(NO_3)_2$: 12.6) (Gustin et al., 2015).

Predominant vegetation at this site was classified as short grass. In Lyman et al. (2007) and Marsik et al. (2007), α and β values were set at 2 and 10 to investigate the effect on calculated dry deposition velocities under constant environmental

ACPD
15, 12069–12105, 2015

conditions. The first is similar to HONO and the second one to HNO_3. Friction velocity and other meteorological data were extracted from the Eta Data Assimilation System (EDAS) 40 km meteorological model using an interpolation method (NOAA, 2008). Daily mean temperature and RH measurements and EDAS-40 km extraction were highly correlated (r^2 = 0.83–0.95 with slope of 1, p value < 0.001). Wind speed was slightly correlated (r^2 = 0.3 with slope of 0.5, p value < 0.001), which is likely due to poor model simulation.

2.5 Back trajectory calculations

Back trajectories were calculated using the Hybrid Single Particle Lagrangian Integrated Trajectory (HYSPLIT 4.9) with EDAS 40 km, 1000 m starting height. For day and nighttime analysis, the starting times were the Local Standard Time 1100–1300 and 100–300, 24 h simulations. For high-concentration event analyses, trajectories were started for each day at 00:00, 04:00, 08:00, 12:00, 16:00, and 20:00 h, LST. Overall, the uncertainties of back trajectories calculated from HYSPLIT are 20 % of the air parcel traveling distance (Draxler, 2013 ; Gebhart et al., 2005; Stohl, 1998; Stohl et al., 2003). Back trajectories were then analyzed using cluster analysis (Liu et al., 2010).

Sigmaplot 14.0 (Systat Software Inc, San Jose, CA, USA) and Minitab 16.0 (Minitab Inc., PA, US) were used to do t tests and correlation analyses. Comparisons were considered significantly different and correlations considered significant when $p < 0.05$.

3 Results and discussion

3.1 Overall measurements

Seasons are delineated as winter (December, January, and February), spring (March, April, and May), summer (June, July, and August), and fall (September, October and November). A significant seasonal pattern (the seasonal pattern discussion excludes

ACPD
15, 12069–12105, 2015

March 2014) was observed for O_3 being highest in the spring; however, CO concentrations were high in winter due to low boundary layer and biomass burning, and low in summer (Table 1).

Observations from 3 GOM sampling methods showed higher GOM concentrations in spring relative to other seasons; however, the magnitudes were significantly different. Concentrations of GOM measured by cation-exchange membranes in the active system were significantly higher than those measured by Tekran® KCl-coated denuder and nylon membranes that have been reported to be influenced by relative humidity (Huang et al., 2013). It is important to note that Huang et al. (2013) pointed out that the active membrane method collects GOM; therefore, data collected from active system were only compared to GOM measured by the Tekran® system. Mean cation-exchange membrane concentrations were higher than Tekran® derived GOM by 14, 48, 11 and 13 times in the spring, summer, fall and winter, respectively. The higher value in the summer is likely due to higher relative humidity, which facilitates collection of GOM on the cation exchange membrane, and reduces availability or capture of GOM by the denuder (Huang and Gustin, 2015b) (Table 1). The underestimation of GOM concentrations using the Tekran® system is due to lack of efficient collection by the KCl-coated denuder of different compounds, and interferences due to humidity and O_3 exposure (Gustin et al., 2013; Huang et al., 2013; Lyman et al., 2010; McClure et al., 2014; Huang and Gustin, 2015b).

Furthermore, nylon membranes measured higher GOM concentrations than those measured by the Tekran® in spring 2013 when the humidity was low. Nylon membrane retention of GOM has been shown to be influenced by relative humidity (Huang and Gustin, 2015b; Huang et al., 2013). Overall, air concentrations measured by the Tekran® system and meteorological data measured in this study were similar to those measured in 2010 (Peterson et al., 2012). Particulate-bound Hg has the same diel trend as GOM but higher concentrations. This could be due to a positive artifact with GOM being collected instead of PBM (Gustin et al., 2013, 2015).

ACPD
15, 12069–12105, 2015

Understanding the oxidants present in air is important for understanding the potential GOM compounds. Oxidants to consider include O_3, halogenated compounds, and nitrogen compounds. Previous work has reported O_3 concentrations were influenced by halogens in the marine boundary layer, and were higher in early morning relative to the afternoon (Dickerson et al., 1999; Johnson et al., 1990); this diurnal (daily) pattern was due to reactions of O_3 and halogens during high solar radiation (for example: $Br + O_3 \rightarrow BrO + O_2$). The O_3 diurnal pattern at OLF showed higher concentrations in the early afternoon relative to early morning (Fig. 2). This is similar to a typical O_3 diurnal cycle at inland sites. However, halogen related oxidation cannot be ruled out, because based on our analyses of data from one year $\sim 24\,\%$ of the air comes from the marine boundary layer during the day and 60 % during the night.

Based on the Tekran® GOM measurements, Engle et al. (2008) also stated the high GOM concentrations at OLF were related to O_3 and solar radiation and from continental air, not the marine boundary layer. Concentrations of NO were high at 07:00 to local time (LT) due to emission from mobile sources during the rush hour as reported in previous studies (Castell-Balaguer et al., 2012; Song et al., 2011). Precursors of O_3 including NO_x and volatile organic compounds (VOC) (Seinfeld and Pandis, 2006) are emitted in the early morning rush hour ($\sim$ 07:00 LT); as solar radiation increased, photo-chemistry dominants the atmospheric reactions to produce O_3 at noon (peak O_3 delayed approximatey two hours after NO_x peak). However, a bi-modal diel (diurnal-nocturnal) pattern was observed for NO_2 and NO_y (Fig. 2). During the morning and afternoon rush hours, NO_2 is oxidized by OH radical and produces HNO_3; however, in the nighttime, NO is oxidized by O_3 to form NO_2 and then NO_3 can be removed by water vapor condensing to form dew (Seinfeld and Pandis, 2006; Song et al., 2011). It is possible that nitrogen compounds produced at night could react to form GOM compounds not quantified by the denuder (cf. Gustin et al., 2013; see discussion below of GOM compounds measured in ambient air). Therefore, O_3 and NO are consumed during nocturnal conditions, and nighttime peaks of NO_2 and NO_y are observed (Fig. 2). Nighttime planetary boundary layer collapse also enhances the NO_2, NO_y and CO

ACPD
15, 12069–12105, 2015

nighttime peaks, and these could contribute to GOM formation through direct reactions (Gustin et al., 2015; Gustin et al., 2012; Weiss-Penzias et al., 2003) or indirect reactions as nitrogen compounds react with volatile organic compounds. Thus, a variety of oxidants are available for forming GOM from GEM.

A slight peak of SO_2 occurred from 07:00 to 11:00 LT, and then concentrations declined over the rest of day. This pattern is due to mixing associated with the breakup of the nocturnal stratification. The change is not as dramatic as observed in Weiss-Penzias et al. (2011) and this is likely due to flue gas desulfurization being implemented at Plant Crist. In addition, SO_2 has to be transported to the site, and there is limited impact from Plant Crist based on the analyses done in Gustin et al. (2012). Diel concentrations of GOM and PBM peak at noon similar to previous observations (Gustin et al., 2012). However, as discussed above, O_3 at OLF does not follow the diel pattern observed in marine boundary layer; this implies the GOM peak at noon is not related to marine halogen species.

The average GEM/CO ratio was $0.0078 \pm 0.0022\,\mathrm{ng\,m^{-3}\,ppbv^{-1}}$; this ratio was fairly stable over the entire sampling period (see Fig. S1 in the Supplement) and similar to that reported for events by Weiss-Penzias et al. (2011). Looking at the monthly variation, June and July were highest, and significantly higher than September and October. Spring was in the moderate range. The calculated GEM/CO emission ratio in Arkansas (AK), Mississippi (MS), Louisiana (LA) is 6.08×10^{-7} ton ton^{-1}; however, GEM/CO ratio of ambient air is 8.96×10^{-7} ppb ppb^{-1}.

Previous work has concluded GEM/CO ratio is approximately $0.0045\,\mathrm{ng\,m^{-3}\,ppbv^{-1}}$ for Asian long range transport (Weiss-Penzias et al., 2007) and around $\sim 0.001\,\mathrm{ng\,m^{-3}\,ppbv^{-1}}$ for North American emissions and biomass burning in the Pacific and Midwest regions (Choi et al., 2013; Weiss-Penzias et al., 2007). However, GEM/CO ratios in this work were similar to those reported in Gustin et al. (2012).

Looking at the ratios on a finer resolution, the ratios are higher in the mid-day. This is because CO is lower during mid-day due to the higher planetary boundary layer and

ACPD
15, 12069–12105, 2015

pulling in of clean marine boundary layer air while GEM concentrations are high from surface emissions.

3.2 Principal Component Analysis (PCA)

Because of the high percentage of missing and below detection limit data for Hg forms (GEM 0.04 % BDL, 26 % missing; GOM 55 % BDL, 28 % missing; PBM 23 % BDL, 28 % missing), PCA was first done using criteria air pollutant and meteorological data without Hg. However, in order to link the PCA factors to Hg, Hg data were added and factor scores were re-calculated. For these analyses, it must be remembered that the GOM concentrations are biased low and all forms are not collected with equal efficiency. From both analyses, two major factors were resolved (Tables 2 and S1 in the Supplement), including factor 1 that included CO, NO_x, and NO_y, and factor 2 that was correlated with SO_2 and O_3. Factors 3 and 4 were found to be related to temperature, solar radiation, wind speed, and GEM, respectively. The first factor is identified as mobile sources due to CO and NO_x emission from vehicles as discussed above, and this is confirmed by the diel pattern of factor 1 (Fig. S2). The factor score of factor 1 was significantly higher at rush hour than the rest of day. Furthermore, this factor is not associated with any Hg forms (Table 2). This could be due to the lack of capture efficiency of the GOM form present such as $Hg(NO_3)_2$, lack of capture and collection on the PBM unit, and/or low Hg content in fuel. Huang et al. (2010) reported a similar factor pattern for mobile sources, and Landis et al. (2007) stated direct Hg emission from mobile sources is low. Their observations are based on Tekran® system data.

The second factor was fossil fuel combustion mixed with gas phase oxidation which correlated with O_3, SO_2, GOM, and PBM. Huang et al. (2010) clearly separated coal combustion (SO_2, GOM and PBM) and gas phase oxidation (O_3, GOM, and PBM) factors. However, in this study, SO_2 and O_3 peaked at the same time (11:00–13:00 LT, Fig. 2). In this case, it is difficult to use PCA to resolve these two co-varying factors. This factor was correlated with high solar radiation and low humidity (Table 2). In the middle of day high solar radiation, high temperature, and low humidity are typically

ACPD
15, 12069–12105, 2015

observed. High solar radiation would enhance the photo-chemistry and increase the radical concentrations in the atmosphere and accelerate Hg oxidation reactions. In addition, humidity enhances GOM and PBM atmospheric removal processes; therefore, the highest GOM concentrations were found at noon. However, vertical convection during the day needs to be considered and this would bring GOM compounds to the surface from the free troposphere, where concentrations have been demonstrated to be high in the Southeastern United States based on vertical profiles collected by aircraft (Brooks et al., 2014). In addition, there are periods when GOM was high but O_3 was not or GOM was elevated but not SO_2, this suggests that parcels of air in the free troposphere with different chemistry may be influencing the boundary layer in Florida (cf. Fine et al., 2015). The third factor was related to meteorological variation and boundary layer collapse. There is no Hg associated with this factor, and this could be due to it not being measured by the denuder due to high relative humidity.

Back trajectories also supported these conclusions. When factor 2 dominated atmospheric processes (11:00–13:00 LT, Fig. 1) 24 % of trajectories were from the Gulf of Mexico, and the rest of the trajectories were from continental areas. However, during the nighttime (01:00–03:00 LT), ~ 60 % of air was from the marine boundary layer, and only ~ 35 % of air was from continental regions.

The pattern for factor 4 with GEM and wind speed indicates accumulation of GEM nocturnally due to collapse of the boundary layer. Based on the results from PCA and diurnal patterns of criteria pollutants, the Tekran® measured GOM concentrations usually peaked at noon associated with gas phase oxidation; however, halogen related reactions do not appear to be involved based on the ozone diel pattern. In addition, the denuder more efficiently collects halogen-Hg compounds, but this would be inhibited by the high relative humidity in Florida. Also, thermal desorption profiles discussed below point to the presence of $HgCl_2$ and/or $HgBr_2$. Lastly, based on the fact that relative humidity was higher at night, and the recent understanding that relative humidity interferes with collection of GOM, some compounds could be present at night that we are

ACPD
15, 12069–12105, 2015

not measuring. Based on the thermal desorption profiles discussed below $Hg(NO_3)_2$ and $HgSO_4$ were present.

3.3 Elevated pollution event

In spring 2013, there was a time period when high concentrations of all forms of Hg were measured by the Tekran® system, O_3, and CO (Fig. 3), and captured using two-week integrated data. Figure 4 clearly shows that the air masses traveled over Arkansas, Mississippi, and Alabama. The air movement pattern is similar to that found in Gustin et al. (2012) for OLF Class 2 events which had low SO_2 concentrations. Air parcels traveling to OLF moved over the surface (less than 300 m above ground level-agl, Fig. 4). Although there are coal-fired power plants in the upwind area within a 500 km range (Fig. 1), the annual average SO_2 concentration implies that the elevated CO, O_3 and GOM were not from fossil fuel combustion. Gustin et al. (2012) also indicated that the free troposphere impacted OLF. The first few endpoints for these trajectories indicate air parcels entered North America at > 1000 m a.g.l.; therefore, there was transport of some air measured during this time from the free troposphere. Ozone concentrations at this time were also similar to those measured in Nevada in the free troposphere (Gustin et al., 2014). It is important to note that the back trajectories are only for 72 h and the ones that subsided to surface levels in the Midwest were traveling fast. We hypothesize this is a common event in the spring that represents free troposphere transport. Fast transport suggests rapid movement in the free troposphere where reactions in the air that would produce GOM could occur during long range transport, and the chemical composition of this event suggests potential input from Asia as suggested for Florida by Gustin et al. (2012).

3.4 Potential GOM compounds

The standard desorption profiles for GOM compounds obtained by Huang et al. (2013) and Gustin et al. (2015) are compared to those obtained at OLF (Fig. 5). It is impor-

ACPD
15, 12069–12105, 2015

tant to note that we do not know exactly what GOM compounds were being produced by the permeation tubes or desorbed from the nylon filter, and here we refer to the primary material in the permeation tube. Only 10 nylon membrane samples collected a significant amount of GOM based on their bi-weekly detection limit (Fig. 5), and their desorption profiles varied. There were 4 patterns of release observed.

One had a high residual tail that does not match our standard profiles. These occurred on 2 April, 4 September and 21 May 2013. This suggests that in spring there is a compound that is unknown based on current standard profiles. $Hg(NO_3)_2$ was found on 21 May 2013 based on the desorption profile. The second pattern occurred on 19 March and 19 November 2013 and this corresponds to $HgBr_2$ with some residual tail that is again some compound not accounted for.

The third pattern occurred on 7 May and 27 August 2013 and corresponds to $Hg(NO_3)_2$ with a residual tail. The 4th pattern that occurred on 14 January 2014 and 24 September 2013 was associated with $HgSO_4$ and the error bars are small. Lastly, the data collected on 22 and 23 October was noisy and had subtle peaks that correspond with HgO, $Hg(NO_3)_2$, and a high residual tail. It is interesting to note that none of the profiles were similar to $HgCl_2$, the form expected to be released by coal-fired power plants.

Previous studies reported consistent desorption profiles from 3 sites in Nevada and California without significant point sources (Huang et al., 2013). Huang et al. (2013) presented desorption profiles from a highway, agriculture, and marine boundary layer site. The profiles from the marine boundary layer and agriculture impacted site do not show clear residual tails at 185 °C, but the highway impacted site did. In addition, at OLF, a significant amount of GOM (15–30 %) was released after 160 °C; this implies that we are missing one or more GOM compound(s) (Fig. 5). Interestingly, a peak was found in the 9 August 2013 sample at the GEM release temperature. This information indicates GOM compounds at OLF varied with time, and this variation is due to complicated Hg emission sources and chemistry. Unfortunately, given the time resolution of the measurement it is difficult to sort out specific sources using back trajectories.

ACPD
15, 12069–12105, 2015

Atmospheric GOM concentrations measured by the Tekran® system were corrected to those measured by cation-exchange membranes ($HgBr_2$: 1.6, $HgCl_2$: 2.4, $HgSO_4$: 2.3, HgO : 3.7, and $Hg(NO_3)_2$: 12.6). These correction factors were derived by comparing GOM concentrations collected using the Tekran® system relative to the cation-exchange membrane using a laboratory manifold system (Gustin et al., 2015; Huang et al., 2013). These values were used to correct GOM concentrations measured by the in-field Tekran® system. Before the correction, GOM concentrations measured by cation-exchange membranes in the active system and by the Tekran® denuder had a low slope (r^2 = 0.64, n = 21, slope = 0.055, $p < 0.001$); however, after the correction, the slope increased with no correlation (r^2 = 0.12, n = 7, slope = 0.23, $p > 0.05$). The low correlation has several explanations: (1) the portion of GOM released at temperatures higher than 160 °C is not correlated with a specific compound; (2) overlap of the standard curves; and (3) complicated atmospheric chemistry. At OLF, the GOM collected on the nylon membrane is more complicated than those collected at sites in the Western US. The desorption curves from the nylon membranes collected at Nevada were in the range of the standard GOM compounds that have been investigated (Huang et al., 2013). Curves with multiple peaks in this study imply that there were at least 5 GOM compounds collected on the membranes. Alternatively, GOM could be formed or reduced on the membrane through reactions related to HNO_3 or sulfur compounds.

3.5 Passive samplers

Uptake rate of GOM collected by the box passive sampler ranged from 0–1.09 pg h^{-1}. These values are adjusted for the blank that traveled with the samplers. Although these are below the detection limit (1.4 pg h^{-1}) which is 3× the standard deviation of the blank collected during the whole study, since the sampler data was corrected by the blank values, and the standard deviations were in most cases low we still feel the data is good. The data were not statistically different by season (ANOVA one-way rank, p value = 0.38) and below detection limit (1.4 pg h^{-1}). There are 6 cases when the sampling

ACPD
15, 12069–12105, 2015

rate was > 0.5 pg h^{-1}. This suggests at these times a form of GOM was available that would more readily diffuse into the sampler (Fig. S2). Recent work has indicated that the sampler as configured only collects 20 % of the GOM (Huang and Gustin, 2015a).

Dry deposition of GOM measured by surrogate surfaces ranged from 0 to 0.5 ng m^{-2} h^{-1}, and 83 % of GOM dry deposition was higher than detection limit (0.12 ng m^{-2} h^{-1}) (Fig. S3). During two 2-week sampling intervals there were 2 periods when dry deposition was not physically measured. Higher GOM dry deposition was observed in spring relative to winter (ANOVA one-way rank, *p*value < 0.01); GOM dry deposition was slightly lower in summer and fall (not statistically different) than in spring due to high wet deposition and scavenging processes. The GOM dry deposition pattern obtained was similar to that reported by Peterson et al. (2012). However, GOM dry deposition rates were significantly higher in this study than 2010 values (0.2 vs. 0.05 ng m^{-2} h^{-1}). This is due to the correction of 0.2 ng m^{-2} h^{-1} being applied in Peterson et al. (2012) to account for contamination of the Aerohead that has been demonstrated to be unnecessary (Huang et al., 2014). Although the highest GOM dry deposition measured using surrogate surface and GOM concentrations measured using the UNR active system were observed in spring 2013, the value in March 2014 was relatively low. In March 2014, atmospheric conditions were more similar to winter than spring, with low temperatures and high CO concentrations. These results converge from those determined using Tekran® measurements that suggest low GOM concentrations and high deposition velocities, and this is because the denuder measurements are biased low (see Gustin et al., 2015). Hg dry deposition calculated for OLF using a deposition velocity of 2 cm s^{-1} and Tekran® GOM concentrations of 2.5 pg m^{-3} is 1.57 µg m^{-2} yr^{-1}. Deposition using the surrogate surface was 1.9 µg m^{-2} yr^{-1}; the value was ∼ 10.8 % of total Hg wet deposition (17.9 µg m^{-2} yr^{-1}) in 2013. However, the modeled dry deposition (with Tekran air concentrations corrected, $\alpha = \beta = 2 - 10$) ranged from 8.4–23.0 % of total Hg wet deposition. These numbers were higher than those in Peterson et al. (2012) due to the 0.2 ng-blank corrections as discussed above.

ACPD
15, 12069–12105, 2015

Because the measurement periods of active and passive membrane systems were offset by a week, modeled GOM dry deposition fluxes were calculated using GOM concentrations measured by the Tekran® system that were multiplied by a factor of three (cf. Huang et al., 2014). In general, measured Hg dry deposition fluxes were similar to those modeled simulations with modeled GOM dry deposition $\alpha = \beta = 2$ (Table 2) during winter, spring, and fall (see below). However, measured Hg dry deposition was significantly higher than modeled results (both $\alpha = \beta = 2$ and 10) in summer and early fall (Fig. 6) by a fairly consistent amount (Table S2). This indicates there are compounds of GOM in the summer that are poorly collected by the denuder, and this also can help explain the higher wet deposition measured during this season (Prestbo and Gay, 2009). Highest deposition was measured during the spring, when the input from long range transport is greatest (Gustin et al., 2012).

Because of the low GOM concentrations and influence of humidity on the nylon membrane measurements (Huang and Gustin, 2015b), GOM compounds were identified only in one summertime sample, which was $Hg(NO_3)_2$. Measured GOM dry deposition was ~ 6 times higher than both modeled results, and if the Tekran® correction factor of three is considered, membrane-based $Hg(NO_3)_2$ dry deposition flux was ~ 18 times higher than the Tekran® -model-based value. Gustin et al. (2015) indicated $Hg(NO_3)_2$ collection efficiency on cation-exchange membrane zero air was about 12.6 times higher than on Tekran (KCl-coated denuder). This indicates the $Hg(NO_3)_2$ collection efficiency on KCl-coated denuder is lower in ambient air than in zero air, due to interferences with relative humidity and O_3.

However, in May 2013, two samples were dominated by $Hg(NO_3)_2$ that showed lower measured/modeled ratios (2.1–6.0 with Tekran® correction factor). The difference here might be due to ambient air GOM chemistry (a compound that has a different dry deposition velocity), less interference on the denuder surface, or parameters in the dry deposition scheme. In May, GOM concentrations measured by the Tekran® were higher than in summer due to low wet deposition (discussed above); in addition, mean humidity was lower in the spring (Table 1). Therefore, GOM collection efficiency varies

ACPD
15, 12069–12105, 2015

with environmental conditions and leads to inconsistent ratios of modeled/measured GOM dry deposition. The dry deposition scheme needs the Henry's Law constant to determine the scaling factors for specific resistances for different compounds (Lyman et al., 2007; Zhang et al., 2002).

Lin et al. (Lin et al., 2006) stated that the dry deposition velocity of HgO is two times higher than that for $HgCl_2$, due to the different Henry's Law constant. The Henry's Law constants for $HgCl_2$, $HgBr_2$, and HgO presented in previous literature (Schroeder and Munthe, 1998) have high uncertainty, for how these calculations were done is not clear (S. Lyman, Utah State University, personal communication, 2015), and the constants for $Hg(NO_3)_2$ and $HgSO_4$ are unknown. Some researchers considered that GOM is similar to HNO_3($\alpha = \beta = 10$), and some treated GOM as HONO ($\alpha = \beta = 2$) (Castro et al., 2012; Lyman et al., 2007; Marsik et al., 2007); however, using the parameters of HNO_3 could overestimate GOM dry deposition velocities due to the differences of effective Henry's law constants ($HgCl_2 :\sim 10^6$ $HNO_3 :\sim 10^{13}$ $M\,atm^{-1}$).

If the ratios ($HgBr_2 : 1.6$, $HgCl_2 : 2.4$, $HgSO_4 : 2.3$, $HgO : 3.7$, and $Hg(NO_3)_2 : 12.6$) of GOM concentrations measured by the Tekran® and cation-exchange membranes for different GOM compounds (Gustin et al., 2015; Huang et al., 2013) were used to correct Tekran® GOM data in this study, modeled GOM dry deposition (Fig. 6) would not be correlated to measurements. Ratios were measured in the laboratory with charcoal scrubbed air; therefore, the effect of water vapor and ozone were not considered and field measurements would be impacted by environmental conditions. For example, on 12 March 2013 and 12 November 2013 (Fig. 6), GOM was dominated by $HgBr_2$ and $HgCl_2$. Dry deposition of $HgBr_2$ from Aerohead sampler measurements and modeling were close as $\alpha = \beta = 10$; however, modeled and measured $HgCl_2$ dry deposition were matched as $\alpha = \beta = 2$. Average deposition velocity for $\alpha = \beta = 2$ was $0.78\,cm\,s^{-1}$, and for $\alpha = \beta = 10$ is $1.59\,cm\,s^{-1}$, if we assume the model is right. There were three samples that were identified as $Hg(NO_3)_2$ using nylon membranes; however, the ratios of measurement and modeling $Hg(NO_3)_2$ dry deposition were inconsistent over time. In spring, all modeled $Hg(NO_3)_2$ dry deposition values were much higher than measured

ACPD
15, 12069–12105, 2015

values; however, in summer, measured and modeled $Hg(NO_3)_2$ dry deposition were similar as $\alpha = \beta = 5$ (Table 3). If you assume the dry deposition measurements made by the surrogate surfaces are accurate then this demonstrates there are different forms that occur over time and these will have different deposition velocities.

4 Conclusions

Active and passive membrane samplers were applied along with Tekran® Hg and criteria air pollutant measurements to understand GOM chemistry and dry deposition at OLF, Florida, US. Based on the diel pattern in O_3, marine halogen reactions have limited influence on Hg reactions during the day at OLF, and GOM and PBM are produced by local photochemical oxidation, and derived from long range transport and delivered to the surface. During the night and early morning when relative humidity is higher, it is likely that GOM compounds are present that are not being measured by the Tekran® system. The fairly constant high GEM/CO ratio is due to low CO coming from the ocean and GEM re-emission from the soil.

In general, PCA indicated that GOM concentrations were associated with SO_2 and O_3 ambient air concentrations, and this indicates GOM is from fossil fuel combustion and gas phase oxidation probably associated with precursors from mobile sources. Additionally, since the diurnal profiles of GOM and SO_2 profiles are not correlated it is possible that the association with SO_2 reflects down mixing of air above the boundary layer. A pollution event with high GOM but low SO_2 concentrations occurred in spring 2013; the air came from the free troposphere based on back-trajectories analysis. This implies GOM concentrations at OLF are significantly impacted by inputs from the free troposphere as suggested by Gustin et al. (2012), and the chemical forms of GOM in the atmosphere can vary by season.

Five potential different GOM compounds were identified at OLF using nylon membranes with thermal desorption analysis, including $HgBr_2$, HgO, $Hg(NO_3)_2$, $HgSO_4$ and a unknown compound. However, because of the complicated and overlapping des-

ACPD
15, 12069–12105, 2015

orption profiles, detailed understanding of GOM composition is difficult. Comparing modeled and measured Hg dry deposition fluxes also demonstrate there are different forms in air, and this will affect dry deposition velocities. In order to improve our understanding of Hg air-surface exchange, physiochemical properties of different GOM compounds need to be understood.

The Supplement related to this article is available online at doi:10.5194/acpd-15-12069-2015-supplement.

Acknowledgements. The authors thank The Southern Company (project manager John Jansen) for their support and Bud Beghtel for deploying and collecting our membranes and passive samplers at the Pensacola Site. This work was also supported by NSF Grant 1326074 and EPRI. We thank the following students for coordinating shipment of membranes and passive samplers, analyses of the membranes in the lab, and keeping the glassware clean (Keith Heidecorn, Douglas Yan, Matt Peckham, Jennifer Arnold, Jen Schoener, and Addie Luippold).

References

Ambrose, J. L., Lyman, S. N., Huang, J., Gustin, M. S., and Jaffe, D. A.: Fast time resolution oxidized mercury measurements during the reno atmospheric mercury intercomparison experiment (RAMIX), Environ. Sci. Technol., 47, 7285–7294, 2013.

Belis, C. A., Karagulian, F., Larsen, B. R., and Hopke, P. K.: Critical review and meta-analysis of ambient particulate matter source apportionment using receptor models in Europe, Atmos. Environ., 69, 94–108, 2013.

Brooks, S., Ren, X., Cohen, M., Luke, W., Kelley, P., Artz, R., Hynes, A., Landing, W., and Martos, B.: Airborne Vertical Profiling of Mercury Speciation near Tullahoma, 5, Atmosphere, TN, USA, 557–574, 2014.

Caffrey, J. M., Landing, W. M., Nolek, S. D., Gosnell, K. J., Bagui, S. S., and Bagui, S. C.: Atmospheric deposition of mercury and major ions to the Pensacola (Florida) watershed: spatial,

ACPD
15, 12069–12105, 2015

seasonal, and inter-annual variability, Atmos. Chem. Phys., 10, 5425–5434, doi:10.5194/acp-10-5425-2010, 2010.
Castell-Balaguer, N., Tellez, L., and Mantilla, E.: Daily, seasonal and monthly variations in ozone levels recorded at the Turia river basin in Valencia (Eastern Spain), Environ. Sci. Pollut. R., 19, 3461–3480, 2012.
Castro, M. S., Moore, C., Sherwell, J., and Brooks, S. B.: Dry deposition of gaseous oxidized mercury in Western Maryland, Sci. Total Environ., 417–418, 232–240, 2012.
Choi, H.-D., Huang, J., Mondal, S., and Holsen, T. M.: Variation in concentrations of three mercury (Hg) forms at a rural and a suburban site in New York State, Sci. Total Environ., 448, 96–106, 2013.
Dickerson, R. R., Rhoads, K. P., Carsey, T. P., Oltmans, S. J., Burrows, J. P., and Crutzen, P. J.: Ozone in the remote marine boundary layer: a possible role for halogens, J. Geophys. Res-Atmos, 104, 21385–21395, 1999.
Draxler, R.: What are the levels of uncertainty associated with back trajectory calculations in HYSPLIT, NOAA, 2013.
Dvonch, J. T., Graney, J. R., Keeler, G. J., and Stevens, R. K.: Use of elemental tracers to source apportion mercury in South Florida precipitation, Environ. Sci. Technol., 33, 4522–4527, 1999.
Engle, M. A., Tate, M. T., Krabbenhoft, D. P., Kolker, A., Olson, M. L., Edgerton, E. S., DeWild, J. F., and McPherson, A. K.: Characterization and cycling of atmospheric mercury along the central US Gulf Coast, Appl. Geochem., 23, 419–437, 2008.
Fine, R., Miller, M. B., Yates, E. L., and Gustin, M. S.: Investigating the influence of long-range transport on surface O_3 in Nevada, USA using observations from multiple measurement platforms, Sci. Total Environ., accepted, 2015.
Gay, D. A., Schmeltz, D., Prestbo, E., Olson, M., Sharac, T., and Tordon, R.: The Atmospheric Mercury Network: measurement and initial examination of an ongoing atmospheric mercury record across North America, Atmos. Chem. Phys., 13, 11339–11349, doi:10.5194/acp-13-11339-2013, 2013.
Gebhart, K. A., Schichtel, B. A., and Barma, M. G.: Directional biases in back trajectories caused by model and input data, J. Air Waste Manage., 55, 1649–1662, 2005.
Gustin, M. S., Huang, J., Miller, M. B., Peterson, C., Jaffe, D. A., Ambrose, J., Finley, B. D., Lyman, S. N., Call, K., Talbot, R., Feddersen, D., Mao, H., and Lindberg, S. E.: Do we under-

ACPD
15, 12069–12105, 2015

stand what the mercury speciation instruments are actually measuring? Results of RAMIX, Environ. Sci. Technol., 47, 7295–7306, 2013.
Huang, J. and Gustin, M. S: Use of passive sampling methods and models to understand sources of mercury deposition to high elevation sites in the Western United States, Environ. Sci. Technol., 49, 432–441, doi:10.1021/es502836w, 2015a.
Huang, J. and Gustin, M.: Uncertainties of gaseous oxidized mercury measurements using KCl-coated denuders, cation-exchange membranes, and nylon membranes: humidity influences, Environ. Sci. Technol., accepted, 2015b.
Huang, J., Choi, H.-D., Hopke, P. K., and Holsen, T. M.: Ambient mercury sources in Rochester, NY: results from Principle Components Analysis (PCA) of Mercury Monitoring Network Data, Environ. Sci. Technol., 44, 8441–8445, 2010.
Huang, J., Miller, M. B., Weiss-Penzias, P., and Gustin, M. S.: Comparison of gaseous oxidized hg measured by KCl-coated denuders, and nylon and cation exchange membranes, Environ. Sci. Technol., 47, 7307–7316, 2013.
Huang, J., Lyman, S. N., Hartman, J. S., and Gustin, M. S.: A review of passive sampling systems for ambient air mercury measurements, Environmental Science: Processes and Impacts, 16, 374–392, 2014.
Jackson, J. E.: A User's Guide to Principal Components, Wiley, 1991.
Johnson, J. E., Gammon, R. H., Larsen, J., Bates, T. S., Oltmans, S. J., and Farmer, J. C.: Ozone in the marine boundary layer over the Pacific and Indian Oceans: latitudinal gradients and diurnal cycles, J. Geophys. Res-Atmos., 95, 11847–11856, 1990.
Landing, W. M., Caffrey, J. M., Nolek, S. D., Gosnell, K. J., and Parker, W. C.: Atmospheric wet deposition of mercury and other trace elements in Pensacola, Florida, Atmos. Chem. Phys., 10, 4867–4877, doi:10.5194/acp-10-4867-2010, 2010.
Landis, M. S., Stevens, R. K., Schaedlich, F., and Prestbo, E. M.: Development and characterization of an annular denuder methodology for the measurement of divalent inorganic reactive gaseous mercury in ambient air, Environ. Sci. Technol., 36, 3000–3009, 2002.
Landis, M. S., Lewis, C. W., Stevens, R. K., Keeler, G. J., Dvonch, J. T., and Tremblay, R. T.: Ft. McHenry tunnel study: source profiles and mercury emissions from diesel and gasoline powered vehicles, Atmos. Environ., 41, 8711–8724, 2007.
Lin, C.-J., Pongprueksa, P., Lindberg, S. E., Pehkonen, S. O., Byun, D., and Jang, C.: Scientific uncertainties in atmospheric mercury models I: Model science evaluation, Atmos. Environ., 40, 2911–2928, 2006.

ACPD
15, 12069–12105, 2015

Lindberg, S. E., Bullock, R., Ebinghaus, R., Engstrom, D., Feng, X., Fitzgerald, W., Pirrone, N., Prestbo, E., and Seigneur, C.: A synthesis of progress and uncertainites in attributing the sources of mercury in deposition, AMBIO, 36, 19–32, 2007.

Liu, B., Keeler, G. J., Timothy Dvonch, J., Barres, J. A., Lynam, M. M., Marsik, F. J., and Morgan, J. T.: Urban-rural differences in atmospheric mercury speciation, Atmos. Environ., 44, 2013–2023, 2010.

Lyman, S. N. and Jaffe, D. A.: Formation and fate of oxidized mercury in the upper troposphere and lower stratosphere, Nat. Geosci., 5, 114–117, 2012.

Lyman, S. N., Gustin, M. S., Prestbo, E. M., and Marsik, F. J.: Estimation of dry deposition of atmospheric mercury in Nevada by direct and indirect methods, Environ. Sci. Technol., 41, 1970–1976, 2007.

Lyman, S. N., Jaffe, D. A., and Gustin, M. S.: Release of mercury halides from KCl denuders in the presence of ozone, Atmos. Chem. Phys., 10, 8197–8204, doi:10.5194/acp-10-8197-2010, 2010.

Marsik, F. J., Keeler, G. J., and Landis, M. S.: The dry-deposition of speciated mercury to the Florida Everglades: measurements and modeling, Atmos. Environ., 41, 136–149, 2007.

McClure, C. D., Jaffe, D. A., and Edgerton, E. S.: Evaluation of the KCl denuder method for gaseous oxidized mercury using $HgBr_2$ at an in-service AMNet site, Environ. Sci. Technol., 48, 11437–11444, 2014.

Nair, U. S., Wu, Y., Holmes, C. D., Ter Schure, A., Kallos, G., and Walters, J. T.: Cloud-resolving simulations of mercury scavenging and deposition in thunderstorms, Atmos. Chem. Phys., 13, 10143–10157, doi:10.5194/acp-13-10143-2013, 2013.

NOAA: Eta Data Assimilation System (EDAS40) Archive Information, Silver Spring, MD, 2008.

Pancras, J. P., Vedantham, R., Landis, M. S., Norris, G. A., and Ondov, J. M.: Application of EPA unmix and nonparametric wind regression on high time resolution trace elements and speciated mercury in Tampa, Florida Aerosol, Environ. Sci. Technol., 45, 3511–3518, 2011.

Peterson, C., Alishahi, M., and Gustin, M. S.: Testing the use of passive sampling systems for understanding air mercury concentrations and dry deposition across Florida, USA, Sci. Total Environ., 424, 297–307, 2012.

Prestbo, E. M. and Gay, D. A.: Wet deposition of mercury in the U. S., and Canada, 1996–: results and analysis of the NADP mercury deposition network (MDN), Atmos. Environ., 43, 4223–4233, 2009.

ACPD
15, 12069–12105, 2015

Schroeder, W. H. and Munthe, J.: Atmospheric mercury – an overview, Atmos. Environ., 32, 809–822, 1998.
Seinfeld, J. H. and Pandis, S. N.: Atmospheric Chemistry and Physics, John Wiley and Sons, Inc., Hoboken, New Jersey, 2006.
Sexauer Gustin, M., Weiss-Penzias, P. S., and Peterson, C.: Investigating sources of gaseous oxidized mercury in dry deposition at three sites across Florida, USA, Atmos. Chem. Phys., 12, 9201–9219, doi:10.5194/acp-12-9201-2012, 2012.
Sexauer Gustin, M., Amos, H. M., Huang, J., Miller, M. B., and Heidecorn, K.: Successes and challenges of measuring and modeling atmospheric mercury at the part per quadrillion level: a critical review, Atmos. Chem. Phys. Discuss., 15, 3777–3821, doi:10.5194/acpd-15-3777-2015, 2015.
Sexauer Gustin, M., Amos, H. M., Huang, J., Miller, M. B., and Heidecorn, K.: Successes and challenges of measuring and modeling atmospheric mercury at the part per quadrillion level: a critical review, Atmos. Chem. Phys. Discuss., 15, 3777–3821, doi:10.5194/acpd-15-3777-2015, 2015.
Song, F., Shin, J. Y., Jusino-Atresino, R., and Gao, Y.: Relationships among the springtime ground–level NO_x, O_3 and NO_3 in the vicinity of highways in the US East Coast, Atmos. Poll. Res., 2, 374–383, 2011.
Stohl, A.: Computation, accuracy and applications of trajectories – a review and bibliography, Atmos. Environ., 32, 947–966, 1998.
Stohl, A., Forster, C., Eckhardt, S., Spichtinger, N., Huntrieser, H., Heland, J., Schlager, H., Wilhelm, S., Arnold, F., and Cooper, O.: A backward modeling study of intercontinental pollution transport using aircraft measurements, J. Geophys. Res., 108, 4370, doi:10.1029/2002JD002862, 2003.
UNEP: Global Merucry Assessment, 2013 – Sources, Emissions, Releases, and Environmental Transport, UNEP Division of Technology, Industry and Economics, Chemicals Branch International Environment House, 2013.
Weiss-Penzias, P., Jaffe, D. A., McClintick, A., Prestbo, E. M., and Landis, M. S.: Gaseous elemental mercury in the marine boundary layer: evidence for rapid removal in anthropogenic pollution, Environ. Sci. Technol., 37, 3755–3763, 2003.
Weiss-Penzias, P., Jaffe, D., Swartzendruber, P., Hafner, W., Chand, D., and Prestbo, E.: Quantifying Asian and biomass burning sources of mercury using the Hg/CO ratio in pollution

ACPD
15, 12069–12105, 2015

plumes observed at the Mount Bachelor observatory, Atmos. Environ., 41, 4366–4379, 2007.

Weiss-Penzias, P. S., Gustin, M. S., and Lyman, S. N.: Sources of gaseous oxidized mercury and mercury dry deposition at two southeastern U. S. sites, Atmos. Environ., 45, 4569–4579, 2011.

Zhang, L., Moran, M. D., Makar, P. A., Brook, J. R., and Gong, S.: Modelling gaseous dry deposition in AURAMS: a unified regional air-quality modelling system, Atmos. Environ., 36, 537–560, 2002.

Zhang, L., Brook, J. R., and Vet, R.: A revised parameterization for gaseous dry deposition in air-quality models, Atmos. Chem. Phys., 3, 2067–2082, doi:10.5194/acp-3-2067-2003, 2003.

ACPD
15, 12069–12105, 2015

Table 1. Overall seasonal average of air species, GEM, PBM, GOM (measured using three different methods) concentration, GOM dry deposition (DD), and meteorological data at OLF.

	2012 Summer	Fall	Winter	2013 Spring	Summer	Fall	Winter	2014 Mar
Ozone [ppb]	30 ± 15	30 ± 12	29 ± 11	38 ± 12	24 ± 12	26 ± 11	27 ± 10	35 ± 12
CO [ppb]	143 ± 38	161 ± 35	167 ± 41	165 ± 36	139 ± 35	156 ± 33	167 ± 35	183 ± 33
SO_2 [ppb]	0.3 ± 0.4	0.6 ± 1.5	0.4 ± 0.5	0.3 ± 0.5	0.2 ± 0.3	0.4 ± 0.5	0.7 ± 1.2	0.3 ± 0.4
NO [ppb]	0.3 ± 0.7	0.3 ± 0.7	0.3 ± 0.8	0.2 ± 0.5	0.3 ± 0.7	0.3 ± 0.8	0.4 ± 0.8	0.2 ± 0.5
NO_2 [ppb]	2.4 ± 2.4	3.0 ± 2.7	3.0 ± 3.1	2.0 ± 2.3	2.2 ± 2.1	3.1 ± 2.9	3.2 ± 3.0	2.3 ± 2.8
NO_y [ppb]	3.6 ± 2.9	4.3 ± 3.1	4.3 ± 3.6	3.1 ± 2.8	3.2 ± 2.5	4.4 ± 3.3	4.2 ± 3.4	3.6 ± 3.1
GEM [$ng\,m^{-3}$][a]	1.2 ± 0.1	1.2 ± 0.1	1.3 ± 0.1	1.2 ± 0.2	1.1 ± 0.1	1.0 ± 0.1	1.2 ± 0.3	1.2 ± 0.1
GOM [$pg\,m^{-3}$][a]	0.6 ± 1.3	1.1 ± 2.8	1.0 ± 2.2	2.9 ± 5.1	0.5 ± 1.0	1.1 ± 2.1	1.3 ± 2.5	2.0 ± 3.6
PBM [$pg\,m^{-3}$][a]	2.4 ± 2.6	3.6 ± 3.8	7.3 ± 8.7	5.9 ± 6.8	2.3 ± 2.0	2.9 ± 2.3	4.9 ± 5.3	4.0 ± 3.4
GOM [$pg\,m^{-3}$][b]	–	–	–	43 ± 110	24 ± 57	14 ± 18	17 ± 23	24 ± 15
GOM [$pg\,m^{-3}$][c]	–	–	–	4 ± 10	0.4 ± 1.3	1.2 ± 1.1	0.6 ± 0.6	0.6 ± 0.5
GOM DD [$ng\,m^{-2}\,h^{-1}$]	0.24 ± 0.20	0.17 ± 0.12	0.15 ± 0.06	0.40 ± 0.23	0.20 ± 0.13	0.13 ± 0.18	0.20 ± 0.50	0.14 ± 0.04
WS [$m\,s^{-1}$]	2.1 ± 1.2	2.1 ± 1.0	2.8 ± 1.7	2.9 ± 1.8	2.0 ± 1.1	2.1 ± 1.1	2.5 ± 1.3	2.5 ± 1.5
TEMP [°C]	26 ± 3	19 ± 6	14 ± 6	18 ± 6	26 ± 3	20 ± 7	11 ± 7	14 ± 5
RH [%]	83 ± 14	76 ± 18	79 ± 19	73 ± 21	84 ± 13	77 ± 17	76 ± 23	78 ± 21
SR [$w\,m^{-2}$]	230 ± 302	193 ± 271	121 ± 199	266 ± 304	210 ± 278	175 ± 255	129 ± 212	182 ± 278
Precipitation [mm]	637	186	385	223	1010	254	357	183

[a] Tekran data
[b] Cation-exchange membrane data
[c] Nylon membrane data

ACPD
15, 12069–12105, 2015

Table 2. Factor loading of the principal component analysis with Hg data. Bold numbers are the variables that are considered significantly correlated.

4 factors	1	2	3	4
ozone	−0.36	0.67	−0.05	−0.18
CO	0.59	0.09	0.39	0.01
SO2	0.22	0.50	0.12	0.23
NO	0.74	0.09	−0.35	−0.09
NO2	0.86	−0.20	0.21	0.08
NO_y	0.95	−0.07	0.12	0.06
GEM	0.03	0.06	0.12	−0.84
GOM	−0.03	0.65	0.07	0.05
PBM	−0.02	0.52	0.46	−0.19
WS	−0.35	0.18	−0.25	−0.58
TEMP	−0.23	0.00	−0.78	0.09
RH	0.07	−0.86	0.01	0.05
SR	−0.05	0.66	−0.57	−0.13
Explained portion	22 %	21 %	12 %	9 %

ACPD
15, 12069–12105, 2015

Table 3. The modeled (multiple-resistance model) and measured (surrogate surfaces) GOM dry deposition ($ng\,m^{-2}\,h^{-1}$), GOM concentrations used to calculate for modeled results are from the Tekran® data and corrected by compounds' corresponding ratios from Gustin et al. (2015). The sample with unknown compound is used the Tekran® data with correction factor of three (average ratio). The tentative GOM compounds are identified from nylon membrane results.

Start date	Tentative GOM compound	Measured GOM dry deposition flux	Modeled GOM dry deposition $\alpha = \beta = 2$	Modeled GOM dry deposition $\alpha = \beta = 5$	Modeled GOM dry deposition $\alpha = \beta = 7$	Modeled GOM dry deposition $\alpha = \beta = 10$
12 Mar 2013	$HgBr_2$	0.50 ± 0.06	0.34	0.49	0.54	0.58
26 Mar 2013	unknown	0.40 ± 0.11	0.34	0.47	0.52	0.56
30 Apr 2013	$Hg(NO_3)_2$	0.50 ± 0.13	1.21	1.67	1.81	1.95
14 May 2013	$Hg(NO_3)_2$	0.40 ± 0.09	1.19	1.69	1.88	2.07
20 Aug 2013	$Hg(NO_3)_2$	0.15 ± 0.07	0.10	0.14	0.16	0.17
11 Dec 2013	$HgCl_2$	0.08 ± 0.03	0.11	0.16	0.17	0.19
1 Jul 2014	$HgSO_4$	0.19 ± 0.03	0.18	0.24	0.27	0.29

ACPD
15, 12069–12105, 2015

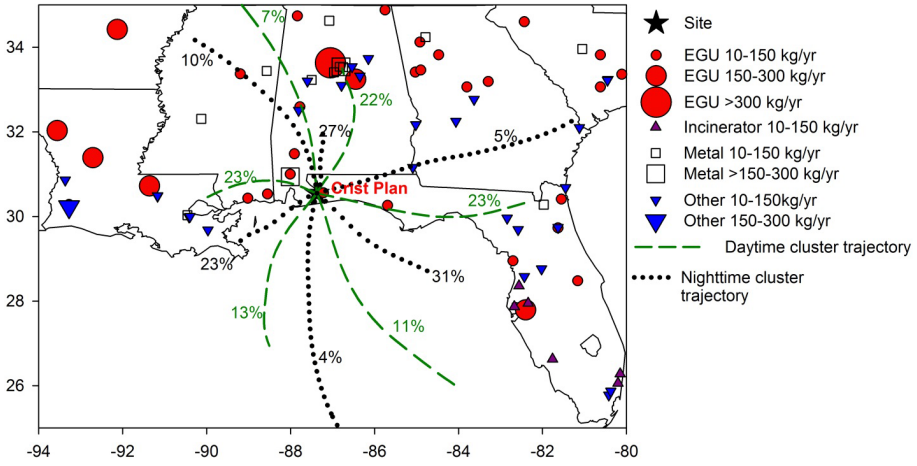

Figure 1. Sampling site and point sources (NEI, 2011) map. Cluster trajectories for daytime (11:00–13:00) and nighttime (01:00–03:00).

ACPD
15, 12069–12105, 2015

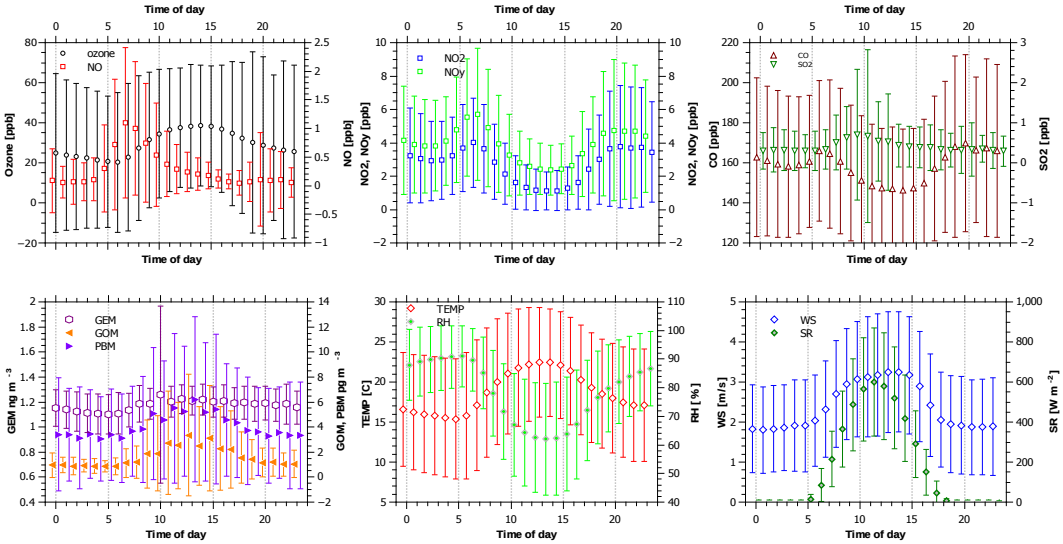

Figure 2. Diel patterns of all air species, mercury forms, and meteorological data. The dot and whisker represent mean and 1 standard deviation, respectively.

ACPD
15, 12069–12105, 2015

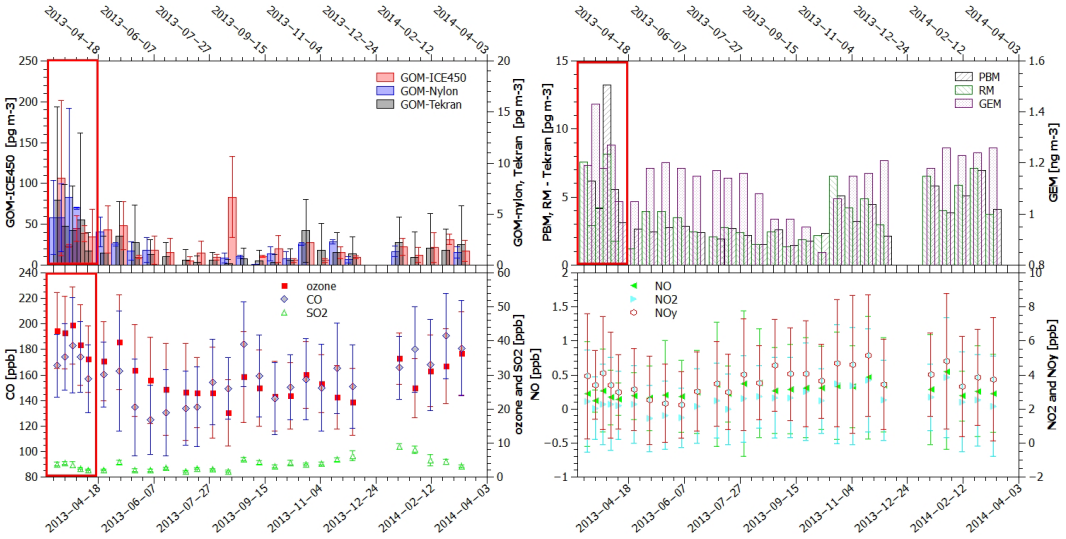

Figure 3. Temporal variation of all air species (mean ± standard deviation, bi-week average), red rectangle indicate a polluted event with high Hg, CO, and ozone concentrations.

ACPD
15, 12069–12105, 2015

Understanding the chemical forms of gaseous oxidized mercury in Florida

J. Huang et al.

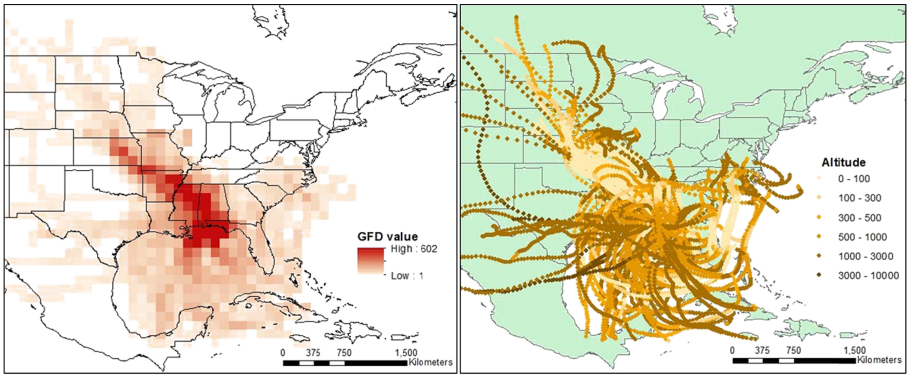

Figure 4. Results of gridded frequency distribution (left), light color indicates less endpoints in a grid. Altitude of 72 h trajectories during the polluted event (12 March 2013–2 April 2013), light color represents low altitude.

ACPD
15, 12069–12105, 2015

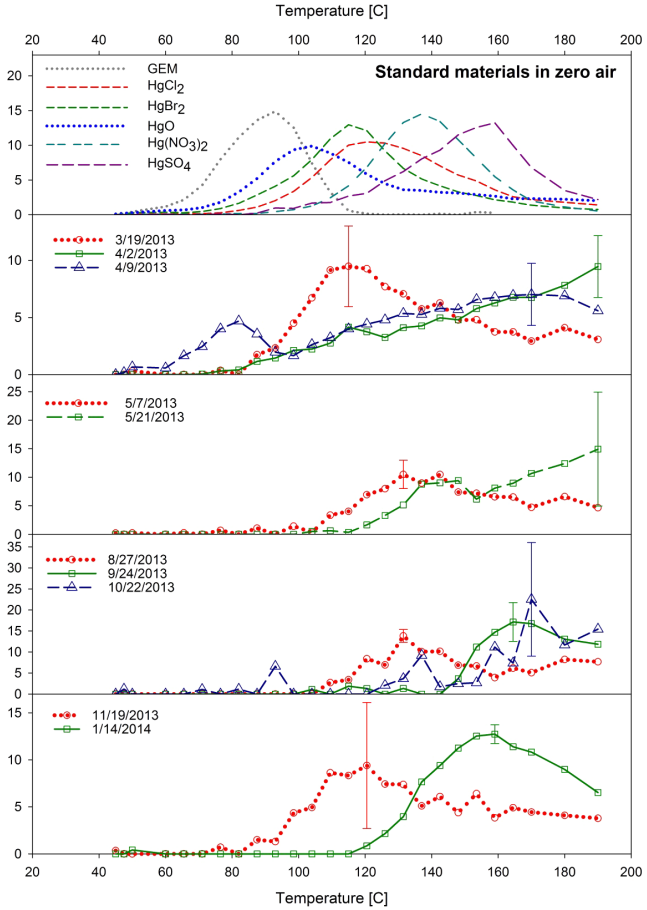

Figure 5. Desorption profile from nylon membranes with standard materials in laboratory investigation (top) and field measurements. Whisker is 1 standard deviation, and only present in the desorption peak.

ACPD
15, 12069–12105, 2015

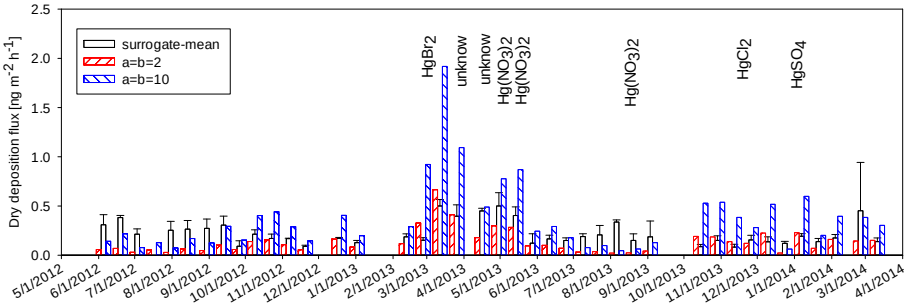

Figure 6. Measured and modeled GOM dry deposition fluxes, Tekran® data (correction factor of three) were used with multiple resistance models ($\alpha = \beta = 2$ and 10). Tentative GOM compounds were determined using the results from nylon membranes desorption.

ACPD
15, 12069–12105, 2015